nature nanotechnology

REVIEW ARTICLE

PUBLISHED ONLINE: 6 APRIL 2017 | DOI: 10.1038/NNANO.2017.45

Imaging modes of atomic force microscopy for application in molecular and cell biology

Yves F. Dufrêne[1]*, Toshio Ando[2], Ricardo Garcia[3], David Alsteens[1], David Martinez-Martin[4], Andreas Engel[5], Christoph Gerber[6] and Daniel J. Müller[4]*

Atomic force microscopy (AFM) is a powerful, multifunctional imaging platform that allows biological samples, from single molecules to living cells, to be visualized and manipulated. Soon after the instrument was invented, it was recognized that in order to maximize the opportunities of AFM imaging in biology, various technological developments would be required to address certain limitations of the method. This has led to the creation of a range of new imaging modes, which continue to push the capabilities of the technique today. Here, we review the basic principles, advantages and limitations of the most common AFM bioimaging modes, including the popular contact and dynamic modes, as well as recently developed modes such as multiparametric, molecular recognition, multifrequency and high-speed imaging. For each of these modes, we discuss recent experiments that highlight their unique capabilities.

The invention of atomic force microscopy (AFM) in 1986[1] is a milestone in the history of nanotechnology[2] and created new opportunities in physics, chemistry, biology and medicine. The technique contours a surface by controlling a conglomerate of forces acting between a tiny probe and the surface. Atomic-scale imaging was obtained within a year of invention[3], but it took a few more years before atomic imaging of nonconductive surfaces in vacuum was achieved. At the same time, the technique started to be adapted to work over a vast temperature scale and in almost every environment[2,4–6]. The ability to investigate surfaces with an exceptional signal-to-noise ratio at subnanometre resolution triggered the development of a range of AFM-related techniques, which used a variety of probes to locally sense interactions and manipulate matter[2,7]. The unique flexibility of AFM to image, probe and manipulate materials made it the most versatile instrument in nanoscience and nanotechnology, and stimulated numerous discoveries and technologies[2]. The possibility to operate in liquid environments and at ambient temperature moved AFM towards biology, and led to the analysis of biomolecules and cells at (sub-)nanometre resolution[4–6,8,9].

To address the wide complexity of biological systems, which can range from nucleic acids and proteins to cells and tissues, a variety of AFM modes have been created over the years (Fig. 1). Major advances in high-resolution imaging have also been achieved in complementary methods, including super-resolution microscopy and cryo-electron microscopy, which enrich the imaging toolbox now available to molecular and cell biologists (Table 1). Many reviews have been published in the past two decades that describe the use of certain AFM imaging modes to characterize biological systems[9–14]. Here, we aim to provide an overview of the diverse range of imaging modes currently available. We survey the significant steps that led to the establishment of AFM as a powerful technique in molecular and cell biology, and, for each AFM imaging mode, we outline the biological systems they can be preferably applied to, their current limitations and their future opportunities.

Imaging native biological systems in liquid

The key breakthrough that led to biological AFM was the development of an optical detection system, followed by the design of a fluid chamber, enabling imaging in buffer solution and thus maintaining the native state of the biological system[4,15]. The first AFM imaging mode invented, contact mode, raster scans a tip over the sample and adjusts pixel-by-pixel the height of the tip so that the force applied to the sample is kept constant (Fig. 2a). The resulting height image resembles the sample topography with the resolution depending on the radius of the tip, the sample corrugation, the physical properties of the sample and how precisely the feedback system contours the tip over the soft biological sample.

Shortly after introducing the first commercially available AFM, biological specimens imaged included animal cells[16,17], cell membrane patches and membrane proteins[18–20], DNA and RNA[21], and lipid films[22,23]. For flat, smoothly corrugated surfaces such as proteins protruding ~1 nm from membranes, contact mode AFM can provide topographs of single membrane proteins at lateral and vertical resolution of <1 nm and <0.1 nm, respectively (Fig. 2b–e) [**Au: Fig. 2b–e correct here?**][20,24,25]. This exceptionally high resolution and signal-to-noise ratio of AFM allowed, for example, the functionally relevant oligomeric state of various water-soluble and membrane proteins to be unravelled[26–30]. Operated in the time-lapse contact mode, AFM visualized the morphological dynamics of cells[16,17], the growth of pathological amyloid fibrils[31], and the enzymatic degradation of DNA[32] and lipid membranes[33], and provided insight into the working principles of bacterial outer membrane pores[34], gap

[1]Institute of Life Sciences and Walloon Excellence in Life Sciences and Biotechnology (WELBIO), Université catholique de Louvain, Croix du Sud 4-5, bte L7.07.06., B-1348 Louvain-la-Neuve, Belgium. [2]Department of Physics, Kanazawa University, Kanazawa 920-1192, Japan. [3]Instituto de Ciencia de Materiales de Madrid, CSIC, Sor Juana Inés de la Cruz 3, 28049 Madrid, Spain. [4]Department of Biosystems Science and Engineering, Eidgenössische Technische Hochschule (ETH) Zürich, Mattenstrasse 28, 4056 Basel, Switzerland. [5]Department of BioNanoscience, Delft University of Technology, Van der Waalsweg 8, 2628 CH Delft, The Netherlands. [6]Swiss Nanoscience Institute, University of Basel, Klingelbergstrasse 80, 4057 Basel, Switzerland. *e-mail: yves.dufrene@uclouvain.be; daniel.mueller@bsse.ethz.ch

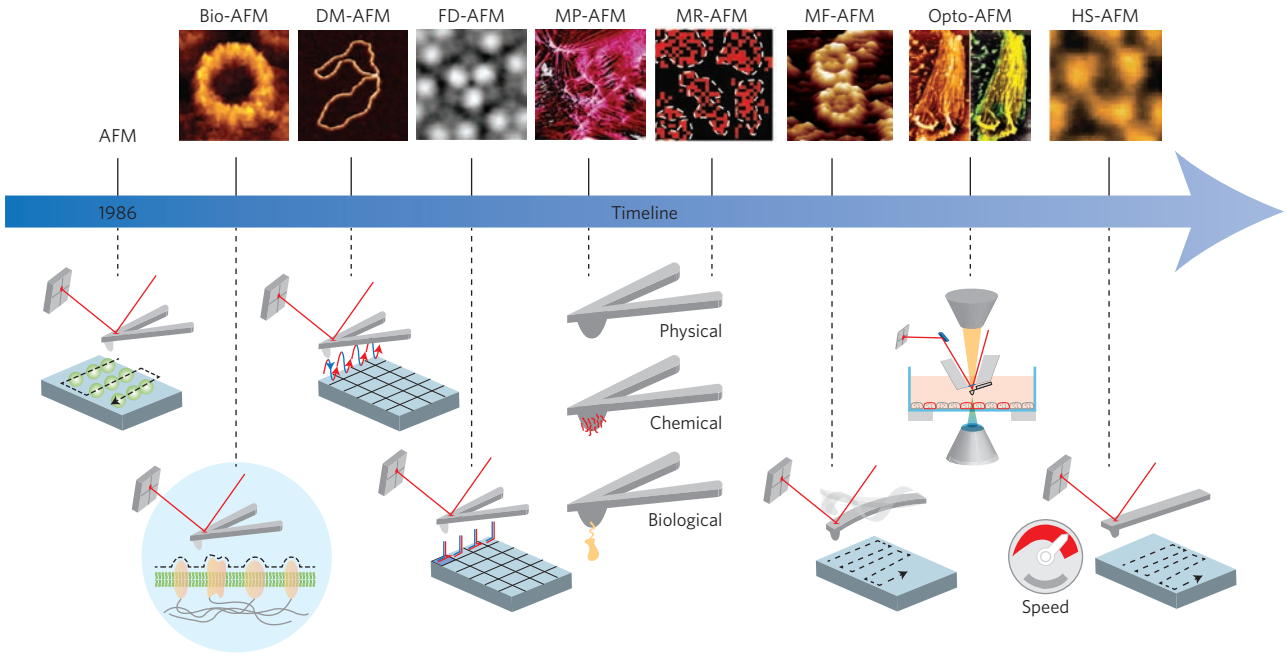

Figure 1 | Timeline of key inventions, starting from the birth of AFM in 1986 to the latest AFM imaging modes in molecular and cell biology. Key inventions developed over the years include: an optical detection system and fluid cell enabling contact mode AFM to operate in aqueous solution (Bio-AFM); dynamic mode AFM (DM-AFM), which oscillates the AFM tip to reduce friction while contouring the biological sample; force–distance curve-based AFM (FD-AFM), which contours the surface of a biological system while recording pixel-by-pixel a full force–distance curve; multiparametric AFM (MP-AFM), which contours the sample while mapping multiple physical or chemical properties; molecular recognition AFM (MR-AFM), which images and maps specific interactions of biological samples; multifrequency AFM (MF-AFM), which contours the sample while oscillating the cantilever tip at multiple frequencies, thus mapping various physical parameters; correlating advanced optical imaging and AFM (Opto-AFM) for the imaging of complex biological systems; high-speed AFM (HS-AFM), which speeds up the image acquisition time by a factor of ~1,000, providing access to dynamic processes in biology. Most modes cross-fertilized each other, ultimately leading to combinatorial AFM. Images adapted from: Bio-AFM, ref. 28, Macmillan Publishers Ltd; DM-AFM, ref. 45, American Chemical Society; FD-AFM, ref. 76, Wiley; MP-AFM, ref. 78, Elsevier; MR-AFM, ref. xx, **[Au: please complete reference number]** Cell Press; MF-AFM, ref. 46, Macmillan Publishers Ltd; Opto-AFM, ref. 145, The Company of Biologists; HS-AFM, ref. 122, Macmillan Publishers Ltd.

junctions enabling intercellular connections between animal cells[35] and nuclear pore complexes[36]. Other exciting examples monitored the insertion of pathological toxins into membranes[37] and the supramolecular architecture of photosynthetic membranes changing in response to light[38]. Such insight allowed static structural models to be complemented with functional dynamics[39].

Although contact mode AFM is widely used to characterize solid substrates, its application to soft biological systems requires expert skills to adjust the force applied to the tip. As a rule of thumb, forces >100 pN should be avoided as they can cause reversible or even irreversible deformations[39]. Dynamic mode imaging (originally termed tapping or oscillation mode) was invented to minimize the friction and the force applied between tip and sample (Fig. 2a,f–h) [**Au: Fig. 2a,f–h correct here?**]. In its simplest application, the cantilever is oscillated close to resonance while scanning across a sample[1]. Ideally, the tip only touches the sample at the very end of its downward movement thus considerably minimizing friction. In close proximity to the sample surface, the interactions between tip and sample change both the cantilever amplitude and resonance frequency allowing them to be used as feedback parameters for contouring fragile biological samples[40,41]. Using the amplitude as feedback is technically simpler because it requires only one feedback loop compared with using frequency as feedback requiring three such loops. Thus, amplitude modulation AFM is currently more often applied than frequency modulation AFM. Besides these two well-known AFM imaging modes, other dynamic modes have been developed that employ different signals as feedback parameters or excite the cantilever at different frequencies simultaneously (see 'Multifrequency imaging')[42]. Importantly, as dynamic modes considerably reduce force and friction between tip and sample, they can be applied to image biological objects that are only weakly adsorbed to supports, such as DNA, single proteins and filaments[43–46]. Dynamic modes also allow highly corrugated objects, such as living cells, to be depicted in their unperturbed state[10]. However, the topographic contrast relies on rather complex interaction mechanisms between the AFM tip and sample. Stiffness, roughness, surface charge and chemistry, or friction of the sample can change the oscillation of the tip and thus alter or even invert the contrast[42]. To record faithful high-resolution images, it can therefore be helpful to image unknown biological systems in the presence of structurally well-characterized reference samples[42,47,48].

Applied to cellular systems, contact and dynamic mode AFM reveal topographs below the resolution limit of conventional light microscopy. The ease of use and the exceptional signal-to-noise ratio quickly raised the hope that AFM would revolutionize live-cell imaging[4,15,16]. Yet, only part of the dream came true. For example, the resolution of animal cell surfaces remained generally limited to ~50–100 nm due to their soft and corrugated nature[9]. In contrast to animal cells, surfaces of microbes, which are mechanically much more rigid and generally smoother, have been routinely imaged approaching a resolution of ~10 nm (refs 49,50). However, polysaccharides of the plasma membrane can contaminate the scanning tip thus changing the image contrast. An elegant approach for imaging living cells and circumventing tip contamination problems is scanning ion conductance microscopy (SICM), which scans a nanopipette over the sample while measuring the ion current[51–53]. The ion current is then used to control the vertical position of the nanopipette and thus to contour the sample. If adjusted properly, this feedback parameter

Table 1 | Comparison of high-resolution imaging techniques in molecular and cell biology.

Technique/feature	Atomic force microscopy	Super-resolution microscopy (STED, PALM, STORM)	Transmission electron microscopy	Scanning electron microscopy
Resolution	≤1 nm–50 nm*	20–50 nm	0.2–10 nm	2–10 nm
Sample preparation and environment	Sample on support; physiological (buffer solution, temperature, CO_2)	Fluorescence labelling; physiological (buffer solution, temperature, CO_2)	Sample on grid; dehydrated (negative stain); vitrified (cryo-electron microscopy)	Freeze/critical point drying and metal shadowing
Artefacts	Tip, force, scanning	Bleaching, toxicity	Dehydration, ice crystal formation, beam damage	Dehydration, metal shadowing, beam damage
Advantages	Imaging under native conditions; no staining, labelling or fixation necessary; high signal-to-noise ratio; assessment of multiple physical, chemical and biological parameters	Access to three-dimensional cellular structures; high spatiotemporal resolution; monitoring biomolecular processes in life cells	Solves atomic structures of proteins; conformational snapshots of proteins and complexes; molecular-resolution structures within the cell	Imaging surfaces of tissues, cells and interfaces at nanometre-scale resolution
Limitations	Restricted to surfaces	Imaging restricted to fluorescence labels	No life processes	No life processes

Whole cell, extracted cellular or synthetic membranes, purified proteins and nucleic acids are considered. *On membrane proteins ≤1 nm can be achieved, on mammalian cells ~50 nm and on microbial cells ~10 nm. STED, stimulated emission depletion; PALM, photoactivated localization microscopy; STORM, stochastic optical reconstruction microscopy. **[Au: please confirm definitions are correct as added]**

can be adjusted to avoid physical contact between pipette and cell. As a result, SICM contours living cellular systems, including hair cells or hippocampal neurons at superior resolution (~50 nm) and in the unperturbed state[52]. Excitingly, SICM can be combined with single-channel patch clamp recordings. However, to apply SICM more widely requires overcoming bottlenecks, including the intrinsically slow imaging process and the convolution of the rather large SICM probe with corrugated cell surfaces.

Last but not least, AFM can be used not only to image but also to manipulate biological samples. The force applied to the AFM tip can simply be adjusted for mechanical manipulation, and the tip can be functionalized with chemical groups to manipulate specific sample regions. Thus, AFM was used to manipulate and dissect cells, chromosomes, viruses, membranes, single nucleic acids and proteins **[Au: OK?]** early on[2,8,54]. The possibility to mechanically manipulate biological systems guided the development of the AFM tip as a nanotool to cut, pick up, release or sculpt biomolecules at nanometre precision and, very recently, even to control the division of animal cells[55–58].

From force–distance curves to multiparametric imaging

The question came up whether AFM can do more than just contouring a surface. A milestone was the realization that, simultaneously with structural imaging, AFM is able to probe biophysical properties. Initially, such properties were measured by approaching the AFM tip to and retracting it from the biological sample while recording single force–distance (FD) curves[59]. Approach FD curves can quantify the height, surface forces and mechanical deformation of the sample, or derive its elastic modulus and energy dissipation. Retraction FD curves allow adhesion forces to be measured (Fig. 3a). To reliably characterize the properties of the sample implies precisely controlling the interaction between tip and sample, thus requiring AFM tips with well-defined geometry and surface chemistry. Sophisticated commercial micro- and nanomachined cantilevers and tips are now available, which are customized in terms of shape, tip radius, and physical and chemical properties. As further discussed below, several imaging modes have been developed to extract the sample properties while imaging the sample[5,60–63]. A versatile and widely distributed approach among these is the FD curve-based imaging mode[13,64,65], which, pixel-by-pixel, approaches and retracts the AFM tip to locally measure forces (Fig. 3b).

Modern FD curve-based AFMs (FD-based AFMs) acquire several hundreds of thousands of FD curves while imaging the biological sample[13]. As each FD curve locally quantifies physical properties and interactions, this information can be directly mapped to the sample topography (Fig. 3c). FD-based AFM thus opens the door to imaging complex biological systems and to simultaneously quantifying and mapping their intrinsic physical properties, including elasticity and adhesion (Fig. 3d,e). Although AFM provides an absolute measurement of the tip position (x, y, z), it is often a challenge to determine the exact contact point between tip and sample (zero separation), particularly when long-range surface forces, surface roughness and deformation of the soft biological sample play roles. Knowledge of the contact point is needed to differentiate surface forces from the mechanical deformation of the soft cell. However, for most applications, linearly extrapolating the contact region to zero force is sufficiently accurate (Fig. 3b).

Currently, the most widely used application of FD-based AFM is the mapping of the mechanical properties of biological systems. This is important because pertinent cellular functions rely on mechanical properties. Pioneering contributions applied the method to image and mechanically map drug-induced changes of the cytoskeleton of fibroblasts[66] and to spatially map the stiffness of the actomyosin cortex of adherent cultured cells during cell division[67] (Fig. 3d). Mapping the viscoelasticity of non-tumourigenic cells and breast tissues showed that they are less deformable compared with cancerous cells and malignant breast tissues, respectively[68,69]. This led to the conclusion that diseased cellular systems show considerably altered mechanical properties. Imaging and mechanically mapping yeast cells (*Saccharomyces cerevisiae*) revealed a substantial stiffening of the chitin-accumulating bud scar compared with the surrounding cell wall[70].

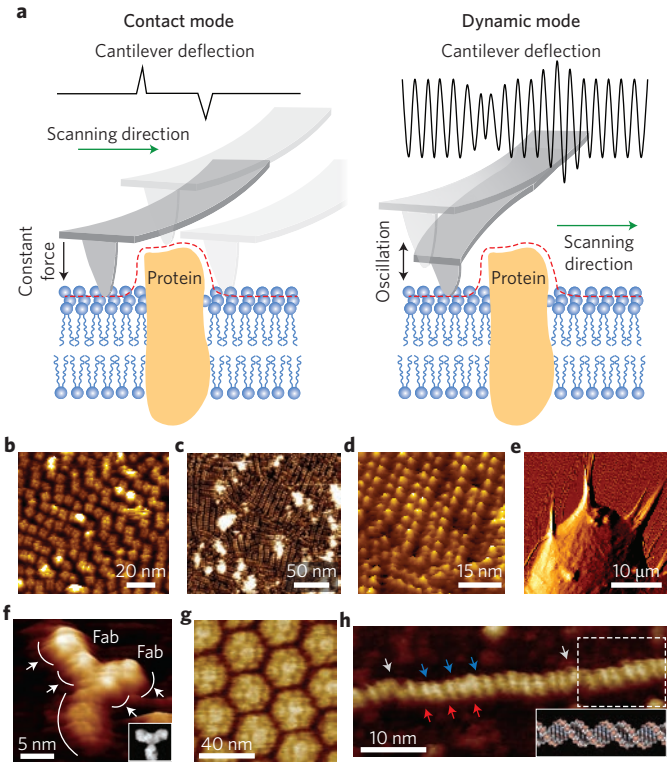

Figure 2 | AFM-based imaging of native biological systems to molecular resolution. a, Basic principles of contact (left) and dynamic (right) AFM imaging modes. In contact mode, the cantilever deflection is kept constant (constant force) by adjusting the relative height between tip and sample. A topographic height change alters the cantilever deflection, which a feedback loop corrects by adjusting the tip–sample distance. The dynamic mode oscillates the cantilever close to or at resonance frequency. Height changes alter the cantilever oscillation, which is used to adjust the tip–sample distance. **b**–**e**, Contact mode AFM topographs. **b**, Cyclic nucleotide-regulated potassium channels (MlotiK1) reconstituted into lipid membranes. **c**,**d**, Rows of densely packed rhodopsin dimers distributed in the native disc membrane extracted from rod outer segments of the eye. **e**, Image of a living SAOS-A2 cell bundling and pulling collagen fibrils coating a substrate. To maximize contrast, the exemplified image shows the deflection of the cantilever, which changes while contouring the sample. **f**–**h**, Dynamic mode AFM topographs. **f**, An IgG antibody absorbed to mica and visualized with frequency modulation mode. **[Au: please provide a brief description of the inset image, define Fab and explain the arrows]** **g**, Single brome mosaic viruses packed in a crystalline assembly. **h**, Circular plasmid DNA imaged in buffer solution by frequency modulation AFM. **[Au: please provide a brief description of the inset image and explain the red and blue arrows and dashed box]** Panels adapted from: **b**, ref. 148, PNAS; **c**,**d**, ref. 30, Macmillan Publishers Ltd; **e**, ref. 147, Elsevier; **f**, ref. 46, Macmillan Publishers Ltd; **g**, ref. 146, Elsevier; **h**, ref. 45, American Chemical Society.

Two interconnected issues in FD-based AFM are the lateral and temporal resolutions. In modern AFMs, the lateral resolution is mainly related to the tip radius, the tip–sample drift, the distance dependence of the tip–sample interaction, imaging force and the properties of the biological sample. Long-range surface forces interacting over several tens of nanometres reduce the resolution at which these interactions can be localized. Technically, when recording an AFM image at a certain frame size, the number of pixels recorded determines the theoretically approachable resolution. However, the amount of pixels and thus the amount of force curves collected per FD-based AFM image is limited by the data acquisition time. In the early days of FD-based AFM[64,65], the time required for recording a single force curve was between ~0.1 and 10 s, and the time needed to acquire a FD-based AFM image of 32 pixels × 32 pixels ranged from ~2 min to ~3 h. Until recently, this slow imaging speed strongly limited the use of FD-based AFM imaging in biology, but the introduction of faster piezo elements, feedback loops, data acquisition systems, oscillation modes changing the tip–sample distance[71], and tailored cantilevers reducing hydrodynamic drag[72–75] largely solved this problem.

As a consequence, nowadays FD-based AFM can record 512 pixels × 512 pixels multiparametric images of native biosystems with a resolution approaching 1 nm, within time ranges of 15–30 min (ref. 13). For instance, the method can image even individual membrane proteins in their native state at ~1 nm resolution and simultaneously map the mechanical properties of their secondary structures[76] and of interfacing lipids[76]. FD-based AFM also mapped the mechanical properties of heterogeneous lipid membranes[77] and correlated the mechanical properties of human keratinocytes[78] and bacteria[79,80] to their morphology and state. Applied to viruses, FD-based AFM has shed new light on the relationship between the structural, functional and mechanical properties of herpes simplex viruses[54], bacteriophages[80,81], southern bean mosaic viruses[82] and parvovirus minute viruses[83]. Excitingly, FD-based AFM can map various molecular and surface forces from the micro- to nanometre scale, including complex and heterogeneous biological systems[84,85]. We are now beginning to understand the time dependence of mechanical interactions, and we can measure, for example, the strength of chemical bonds[86], as well as the mechanical response of biological materials under different loading rates[62,87]. Although technological improvements have considerably reduced the acquisition time of FD-based AFM images, it remains an important challenge to further increase the imaging speed so that the multiparametric complexity of dynamic molecular and cellular processes can be fully addressed.

Molecular recognition imaging

Soon after introducing FD-based imaging, the idea to map specific chemical and biological properties was born[88–91]. This approach requires tip–sample interactions to be known, which is facilitated by functionalizing AFM tips with specific chemical groups or ligands[89,90]. FD curves then allow the adhesion and mechanical strength of specific bonds formed between tip and sample to be measured[92,93]. Accordingly, FD-based AFM can map such specific forces while imaging the biological system[11,13]. Chemical tips can be obtained by functionalizing gold-coated tips with self-assembled alkanethiol monolayers terminated by specific functional groups[88]. Alkanethiols functionalized with nitrilotriacetate-terminated groups that attach histidine-tagged biomolecules of interest have been used[94]. Silicon tips can be amino-silanized and reacted with polyethylene glycol linkers, which carry benzaldehyde functions to attach peptides or proteins through lysine residues[89].

Using functionalized probes, FD-based AFM could detect and localize specific interactions of biological systems ranging from antibodies to living human cells[11,13,89–91,95]. Biospecific FD-based AFM has proven useful to map receptor sites on animal cells. In an early work, AFM tips bearing the Helix pomatia lectin were used to map N-acetylgalactosamine-terminated glycolipids on group A red blood cells[91]. Since then, receptors mapped on animal cells include vitronectin receptors on osteoblasts[96], prostaglandin receptors on Chinese hamster ovary (CHO) **[Au: definition OK?]** cells[97] and glycosylphosphatidylinositol-anchored proteins in neuronal membranes[98]. In another example, human G-protein-coupled receptors were imaged in membranes while measuring and mapping their single binding events of native and synthetic ligands[99]. By moving the AFM tip in a nonlinear manner, the unbinding forces of the ligands were measured over a very wide loading rate, which allowed the free-energy landscape of receptors binding to ligands

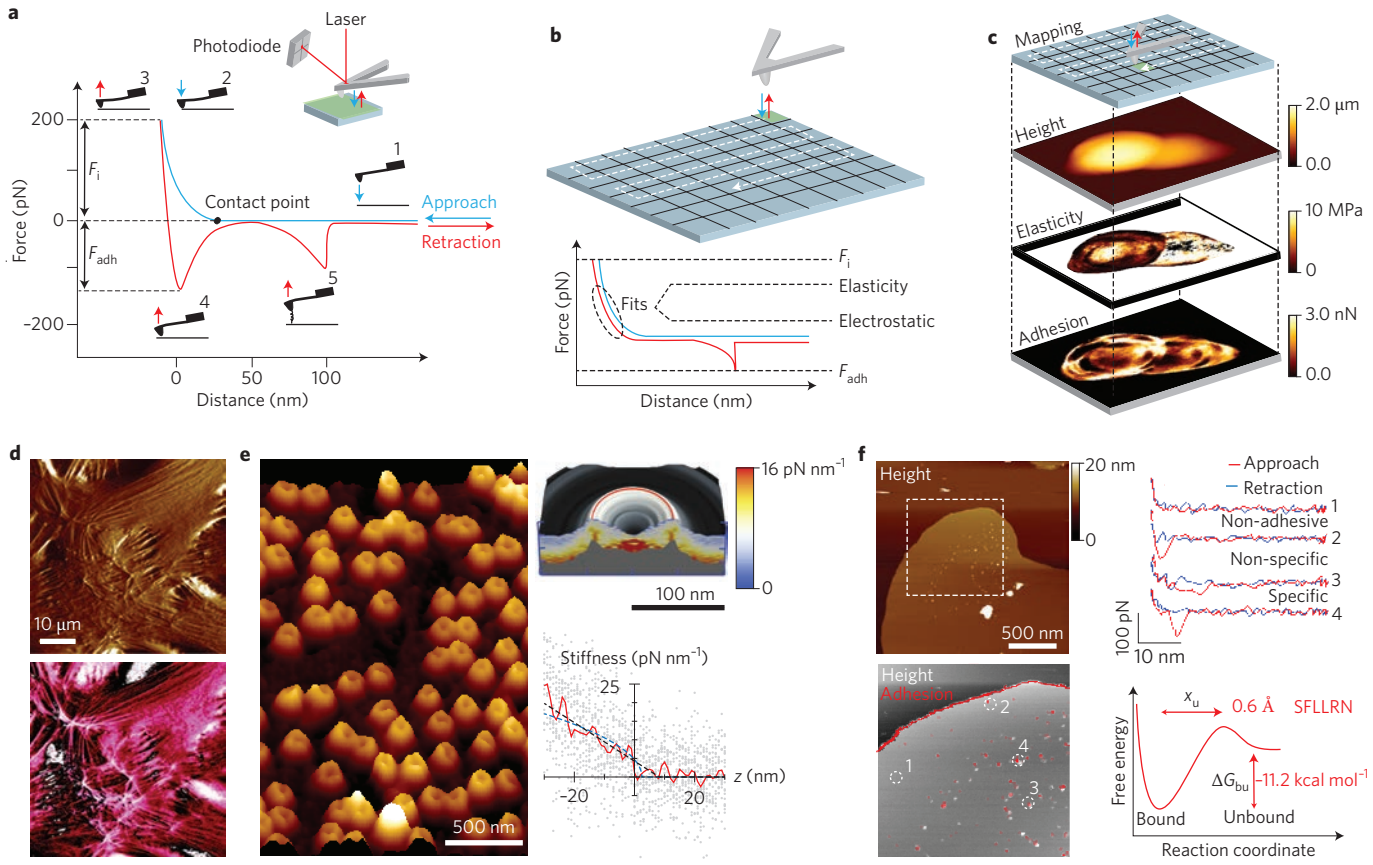

Figure 3 | Force–distance curve-based AFM. a, Principle of recording force–distance (FD) curves by approaching (blue) and withdrawing (red) the AFM tip from the sample. The tip of the cantilever is initially away from the sample (1) to which it is brought into contact (2). During retraction (3) of the AFM tip, adhesive events may occur at different distances due to nonspecific (4) or specific (5) interactions between tip and sample. **b**, FD-based AFM imaging records pixel-by-pixel FD curves while contouring the sample topography. The indentation force F_i is controlled and parameters extracted include the tip–sample adhesion force F_{adh}, or elastic and electrostatic properties (by fitting the curve). Parameters can be displayed as coloured maps and correlated to the topography. **c**, Example of multiparametric FD-based AFM imaging of the elasticity and adhesion of two dividing Staphylococcus aureus cells. **d**, AFM force error (top) and elasticity (bottom) maps **[Au: insertion of 'top' and 'bottom' correct?]** of living HaCaT keratinocytes. **e**, Topography (left, brown coloured) and stiffness map (top right) of nuclear pore complexes from the cytoplasmic surface. The graph (bottom right) shows the stiffness as a function of tip–sample separation recorded close to the centre of the cytoplasmic ring. **[Au: please explain the different coloured lines and the grey dots]** **f**, Top left: topograph of human protease activated receptors 1 (PAR1) in proteoliposomes recorded with a SFLLRN-ligand functionalized tip. Bottom left: overlay of topograph (grey) and adhesive interactions (red) localizes individual receptors binding the ligand. **[Au: please provide a brief explanation of the numbered circles]** Top right: force–distance curves exemplifying unspecific adhesion events (1 and 2) and specific ligand-receptor unbinding events (3 and 4) showing the stretching of the linker tethering the ligand to the AFM tip. Bottom right: free energy landscape of the ligand binding to PAR1 extracted from measuring the rupture force of the ligand-receptor bond at different loading rates. **[Au: please define X_u and ΔG_{bu}]** Panels adapted from: **c**, ref. 79, PNAS; **f**, ref. 99, Macmillan Publishers Ltd. Panels reproduced from: **d**, ref. 78, Elsevier; **e**, ref. 149, Macmillan Publishers Ltd.

to be reconstructed (Fig. 3f). Applied to live bacteria and yeast, the main components of microbial cell walls have been localized and force probed, including peptidoglycans[50], teichoic acids[100] and cell adhesion proteins[84,101]. These studies revealed the heterogeneous distribution of microbial cell surface molecules, which is related to the cell state. In addition, the assembly machinery of bacteriophages was imaged on live bacteria and localized near the septum in soft nanodomains surrounded by the stiffer cell wall[80]. Whereas these applications functionalized the AFM tip with one type of biomolecule, a recent approach functionalized the AFM tip with two different ligands to map two binding sites of human G-protein-coupled receptors[102]. Such application opens the door to AFM-based multifunctional recognition imaging.

A critical issue when analysing adhesion forces detected by FD-based AFM is to proof their specificity and to separate them from unspecific ones. Controls include blocking the specific interactions with antibodies or chemical compounds, and using mutant cells lacking the specific recognition sites. For direct comparison, fluorescently labelled target and mutant cells may be co-cultured, identified by fluorescence microscopy and simultaneously imaged with the functionalized tip. Tip contamination is another problem that needs to be addressed. With complex samples such as living cells, adsorption of loosely bound molecules may quickly change the functionalized tip, making the tip record unknown interactions with the sample. Therefore, before engaging functionalized tips, it is useful to characterize the sample with unmodified tips. Also, one should always keep the applied force below 100 pN.

An alternative to FD-based AFM is topography and recognition imaging (TREC) **[Au: definition OK?]** imaging, which records topography and specific recognition images at a similar speed to contact mode AFM[103,104]. This method was used to map the binding sites of cadherins on vascular endothelial cells[105]. TREC oscillates functionalized tips at very small (5–10 nm) amplitudes while scanning the sample. A specific binding event is then detected via an amplitude change. However, as FD curves are not recorded, quantitative information of the molecular binding events is lacking.

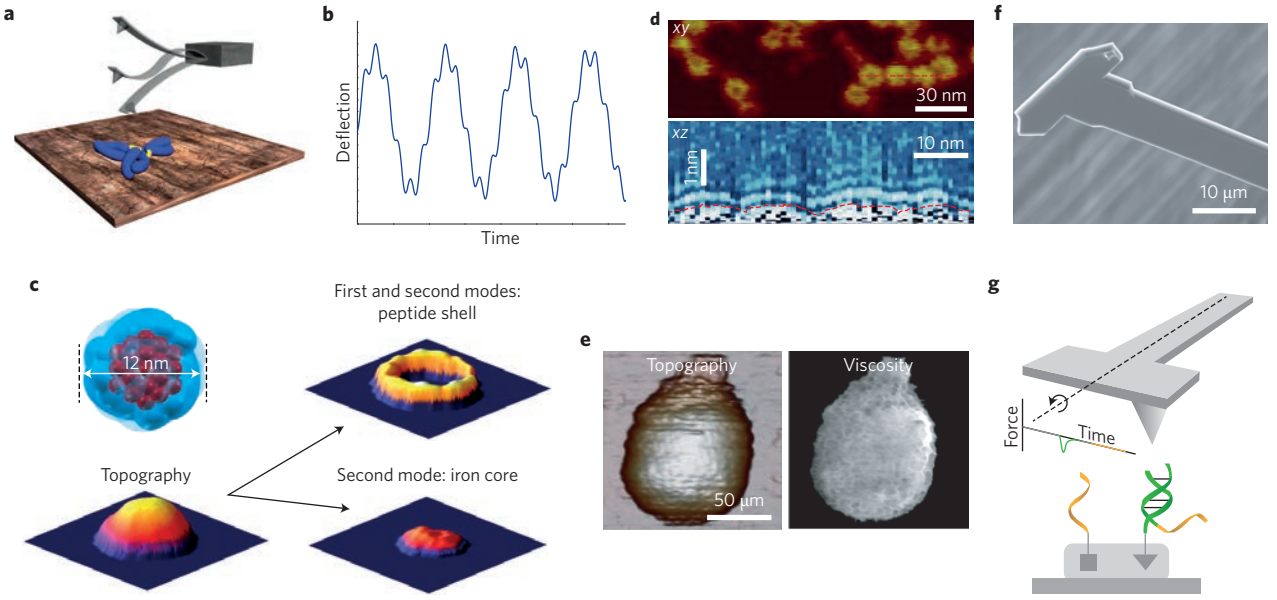

Figure 4 | Multifrequency AFM. a, Scheme of the deflection of the cantilever in bimodal AFM. **[Au: please provide labels for this scheme] b**, Two eigenmodes of the cantilever are excited and detected. Observables associated with both eigenmodes are recorded to determine sample properties such as flexibility, deformation and viscosity. **c**, Separation of short-range mechanical forces and long-range magnetic interactions in ferritin. The first eigenmode contours the topography while the second eigenmode detects long-range magnetic forces. By combining both signals, the iron oxide core and the apoferritin shell are separated in the AFM image. **d**, Top: AFM topograph (*xy* frame) of GroEL proteins. Bottom: vertical profile (*xz* frame, taken along the red dashed line of the topography) of the hydration layers contouring four GroEL molecules. The dashed red line marks the surface of the GroEL molecules. **e**, Multifrequency flexural AFM of a bacteriophage Φ29 mature virion. The virion topography (left) is acquired simultaneously with multiharmonic observables images, from which the viscosity map (right) is shown. Images were recorded applying 100 pN. **f**, False colour electron microscopy image of a T-shaped cantilever designed for torsional harmonic AFM. **g**, Multifrequency torsional harmonics scheme for probing chemical groups of a protein using DNA labels. A DNA strand attached to the tip interacts with target DNA strands. Complementary sequences have identical colours. Panels adapted from: **a**, ref. 42, Macmillan Publishers Ltd; **c**, ref. 150, IOP; **d**, ref. 108, RSC; **e**, ref. 110, RSC; **f**, ref. 60, Macmillan Publishers Ltd. Panel **g** reproduced from ref. 112, Macmillan Publishers Ltd.

Multifrequency imaging

Besides topographic imaging, AFM can map mechanical and functional properties of the biological sample. However, applying modes such as FD-based AFM considerably increases the data acquisition time[13]. Advanced dynamic mode AFM, including frequency or amplitude modulation, or multifrequency mode AFM offer higher frame rates. Recently developed multifrequency AFM modes[42,106], which promise exciting possibilities to study biological systems, are therefore discussed. Multifrequency AFM involves the simultaneous excitation and/or detection of several frequencies of the cantilever motion. These frequencies are usually associated with multiple integers (harmonics) of the fundamental frequency or intrinsic resonance frequencies (eigenmodes) of the cantilever[42]. There are several multifrequency AFM approaches[42]; however, their physical foundations can be quite complex and mostly their theoretical description is still under development. One key issue is to develop analytical expressions that relate the observables (amplitude, phase or frequency shifts) to material properties, such as topography, flexibility, adhesion, stiffness, magnetic or electrostatic[14]. A straightforward explanation of how these methods operate is provided by bimodal AFM, which excites two eigenmodes of the cantilever and measures their observables (Fig. 4a,b). This combination of the first and second eigenmodes multiplies the number of observables to characterize the sample properties by a factor of two and requires just four data points per topographic pixel.

Bimodal AFM has been applied to record topography and flexibility maps of a single IgM antibody at a spatial resolution of ~2 nm, **[Au: OK?]** showing that the uppermost part of the protein complex has an effective Young's modulus of 18 MPa while the antibody domains are much softer (8 Pa)[42,62]. Bimodal AFM has also been used to image ferritin while separating short-range mechanical (~0.5 nm) from long-range magnetic (~5–1,000 nm) forces. The separation of mechanical forces provided by the stabilizing protein shell and of magnetic forces of ferritin is possible because the first eigenmode is more sensitive to short-range repulsive forces while the second eigenmode measured long-range interactions (Fig. 4c)[107]. Imaging of water layers covering the chaperone GroEL at forces <20 pN exemplifies the potential of bimodal AFM to provide novel insight about sample properties (Fig. 4d)[108]. Complementary to this frequency modulation, AFM has also been applied to image hydration layers at the water–lipid interface of lipid membranes[109].

Multiharmonic AFM excites the cantilever with a single frequency while recording multiple harmonics of the flexural or torsional cantilever motion. Initially, this AFM imaging mode has been applied to measure topography and viscoelastic properties of relatively large biological objects, including viruses and cells (Fig. 4e)[110,111]. Torsional harmonics allow the topograph of the sample and the time-varying forces to be recorded by integrating the higher harmonics of the torsional movement. These forces quantify the mechanical properties of the sample, including Young's modulus or adhesion. Torsional harmonics also detect interactions in the microsecond range[75] and measure recognition forces of chemical groups or protein complexes (Fig. 4f,g)[112]. However, torsional harmonic AFM requires the use of specially designed T-shaped cantilevers, which are not yet commercially available. This necessity together with the need to use complex algorithms to analyse the harmonics data is currently limiting wider application of the technique.

Accessing the subsurface morphology of complex biological systems has been a longstanding challenge for AFM. Recently, ultrasonic microscopy and dynamic AFM have been combined

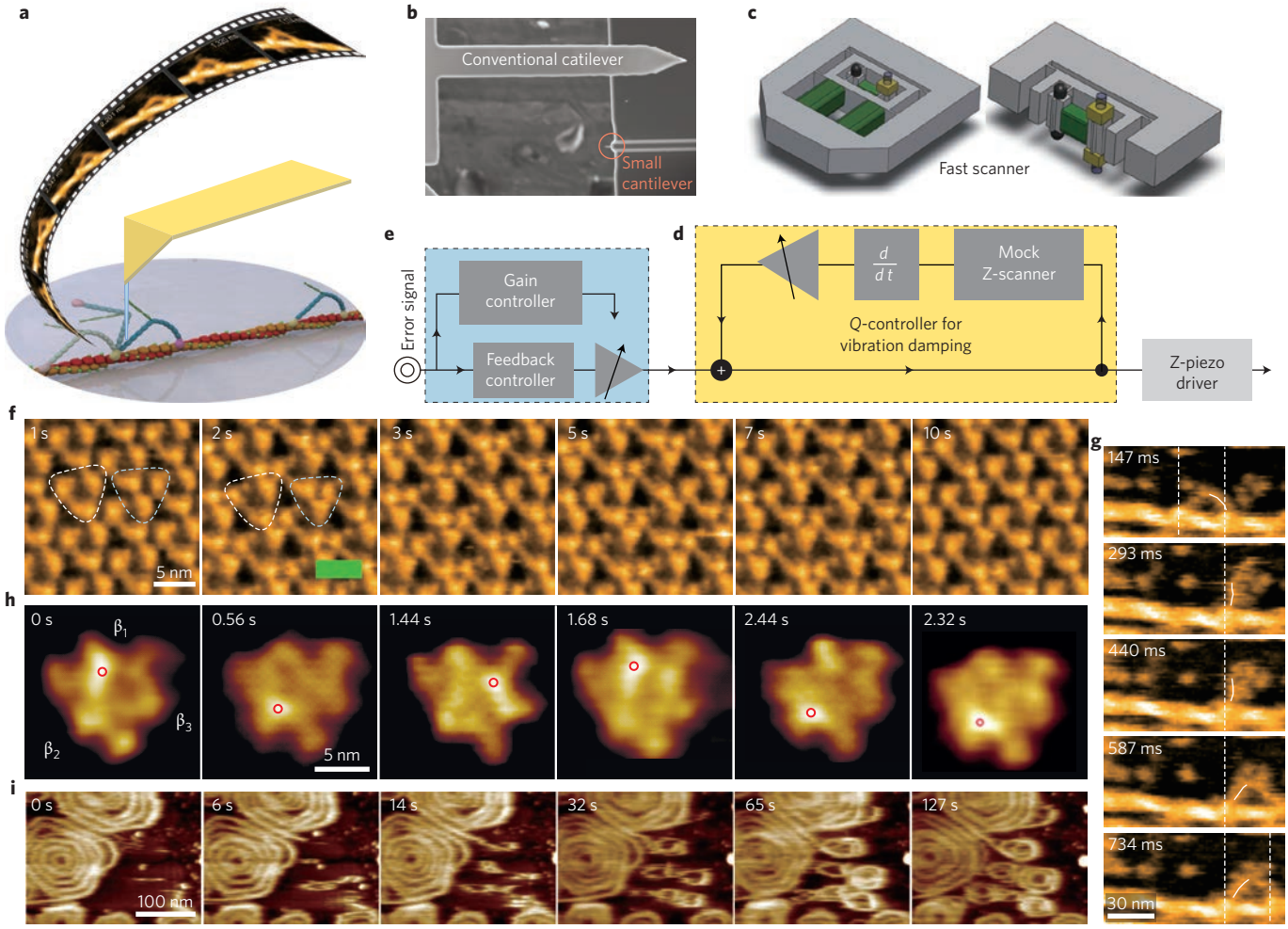

Figure 5 | HS-AFM filming proteins in action. a, Illustration of filming myosin walking along actin filaments. **b**–**e**, Key devices and techniques for HS-AFM. **b**, Small cantilever with high resonant frequency and small spring constant. **c**, Fast scanner suppressing impulses generated by quick displacements of piezoelectric X- and Z-scanners. **d**, Active vibration damping based on *Q*-control with mock Z-scanner. **e**, Feedback controller with automatic gain tuning for low-invasive high-speed imaging without causing tip-parachuting. **f**–**i**, HS-AFM images of proteins in action. **f**, Bacteriorhodopsin in native purple membrane recorded under dark and illumination at 1 frames per second. White triangles indicate bacteriorhodopsin trimers. Blue triangles indicate 'trefoils' that comprise three bacteriorhodopsin monomers, each belonging to an adjacent trimer. Green light was illuminated at 2 s and switched off at 3 s. On illumination, bacteriorhodopsin trimers dilate outwardly, while bacteriorhodopsin monomers contact each other in trefoils. **g**, Myosin V walking unidirectionally along an actin filament, showing forward rotation of the leading lever-arm on trailing head detachment from actin. **[Au: please explain the dashed white lines] h**, Rotorless F_1-ATPase undergoing conformational changes. Red circles indicate the highest positions of the topographs. Since a nucleotide-free β-subunit protrudes higher than ADP- and ATP-bound ones, it is observed that the unbound state rotates anticlockwise. **i**, Spiral filament formation by polymerization of the ESCRT-III protein Snf7 on a supported lipid membrane. Panels adapted from: **f**, ref. 122, Macmillan Publishers Ltd; **g**, ref. 123, Macmillan Publishers Ltd; **h**, ref. 124, AAAS; **i**, ref. 125, Elsevier. **[Au: please check all citations of the panels in this figure are correct and indicate where panel a should be cited]**

to mechanically excite sample and cantilever, which generates mechanical waves that propagate through the biological sample. Waves mechanically interacting with the inside of the sample change amplitude and phase[113,114]. Thus, by using the AFM tip to probe these changes pixel-by-pixel can provide the topography and structures beneath. This method shows potential for the imaging of embedded or buried subsurface structures of animal and plant cells. However, at present, subsurface imaging requires the application of relatively large forces (~100 nN), which questions to what extent the structures imaged are representative of a native unperturbed cell. In addition, the use of delocalized ultrasonic waves to generate images of subsurface structures leaves interpretative challenges and limits the spatial resolution[115]. There is thus progress to be made before this AFM imaging mode will be applicable to a broad audience to address pertinent biological problems.

High-speed imaging of biological processes in real time

Compared with fluorescence microscopy, AFM imaging is limited by its rather slow time resolution. In recent years, however, tremendous technological advances have allowed the imaging speed to be increased, thus offering a means to study dynamic molecular processes by high-speed AFM (HS-AFM). Among AFM components, the slowest is the cantilever. Therefore, to achieve high-speed using amplitude modulation AFM, the cantilever's response time $\tau = Q/(\pi f_0)$ has to be shortened, with Q being the quality factor and f_0 the first resonance frequency of the cantilever in water (Fig. 5b). To increase f_0, while keeping the spring constant k small, small cantilevers (100–140 nm thick, 2–5 μm wide and 9–14 μm long) were developed, thereby approaching f_0 = 100–650 kHz and k = 0.1–0.3 N m^{-1} (refs 72,73). Because the Q value of these small cantilevers approaches ~2 in water, their response time of ~1–6 μs is 40–240-fold shorter

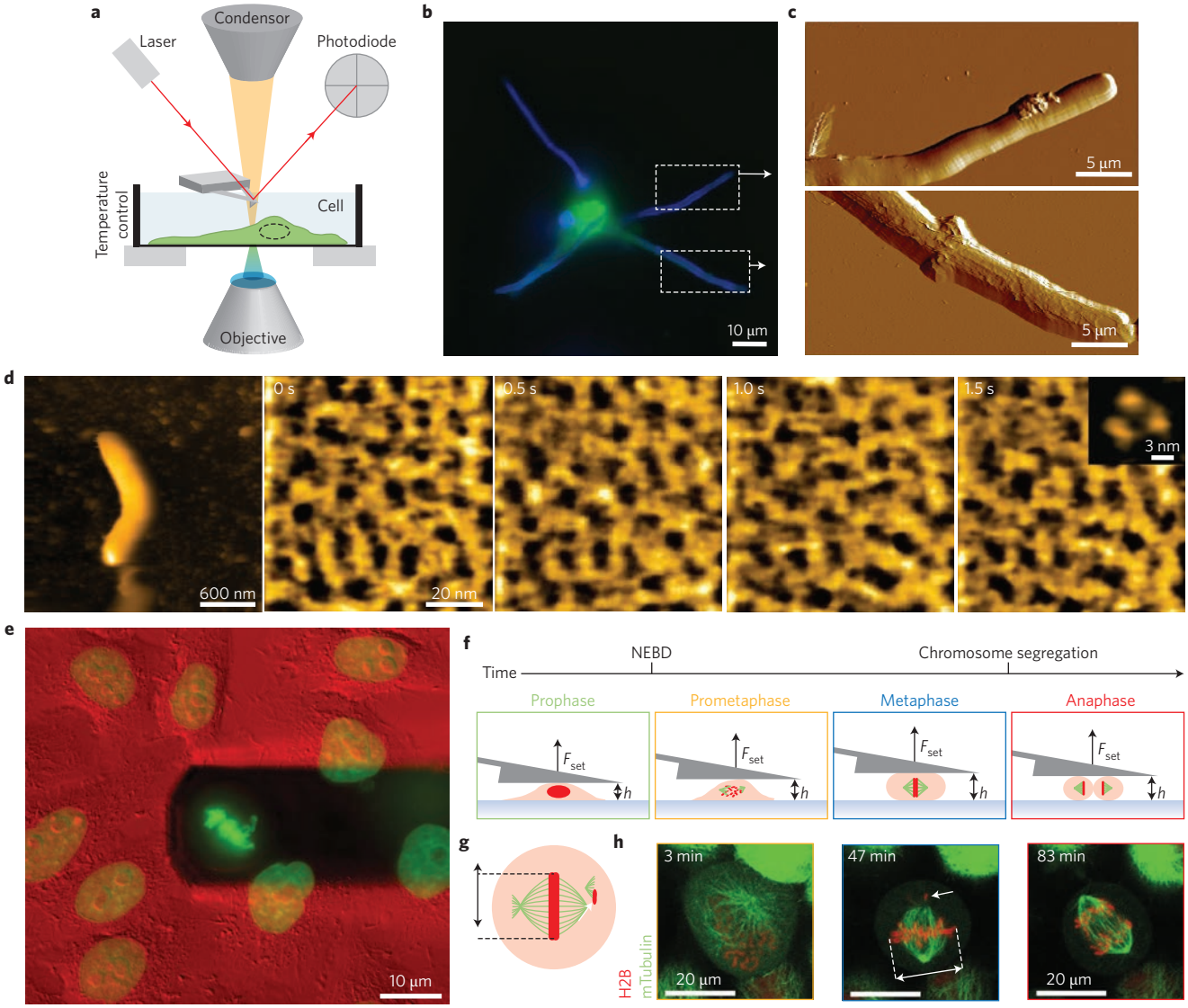

Figure 6 | AFM of cellular systems. a, Schematic setup of an AFM combined with optical microscopy for the characterization of living cells. **b**,**c**, Fluorescence image (**b**) and correlative AFM images (**c**) of a macrophage (green) incubated for 3 h with cells from Candida albicans (blue). Images in panel **c** are enlarged views of the dashed areas shown in the fluorescence image. Internalized (bottom) and externalized (top) hyphae featuring major structural differences. **d**, HS-AFM topographs of the Escherichia coli bacterium. The first topograph shows the entire bacterium, while the following images of the outer membrane show moving net-like structures formed by porin trimers. The inset in the last image shows a single porin trimer. **e**, Mechanical confinement and morphological characterization of mitotic animal cells. The image shows overlaid differential interference contrast and histoneH2B green fluorescent protein (H2B-GFP) images of mitotic HeLa cells. The cantilever (dark shadowed) confines a single mitotic cell in the metaphase to measure the force and pressure generated by the rounding animal cell. **f**, Wedged cantilever applied to confine a mitotic HeLa cell and to mechanically control mitotic progression. Depicted are mitotic phases, spindle microtubules (green), chromosomes (red), nuclear envelope breakdown (NEBD), time (t), and force (F_{set}) and height (h) set by the cantilever. **g**,**h**, Top view of spindle characterization scheme of a confined HeLa cell (**g**) and fluorescence snapshots of microtubules (mTubulin–GFP) and chromosomes (H2B–mCherry) (**h**). Grey double arrows, metaphase plate width; white arrows, stray chromosomes. t = 0, NEBD. Panels adapted from: **a**, ref. 131, American Chemical Society; **e**, ref. 139, Macmillan Publishers Ltd. Panels reproduced from: **b**,**c**, ref. 131, American Chemical Society; **d**, ref. 128, Elsevier; **f**–**h**, ref. 58, PNAS.

than conventional cantilevers. At present, small cantilevers with f_0 = 400–800 kHz and k = 0.1–0.2 N m^{-1} are commercially available. To achieve HS-AFM, it is also important to suppress mechanical vibrations of the Z-scanner, which is moved at much higher frequencies than X- and Y-scanners (Fig. 5c). For this, three approaches were taken; counterbalancing the impulse generated by quick Z-scanner displacements[73], designing robust scanner structures[116,117] and actively damping vibrations based on a Q-control technique (Fig. 5d)[118]. The last component to be noted is a controller that can dynamically tune the feedback gains during imaging to minimize the tip–sample force (Fig. 5e)[119]. The highest possible imaging rate of HS-AFM as a function of various parameters is quantitatively described elsewhere[12].

In the early days of HS-AFM, DNA[72], the GroEL–GroES chaperonin system [**Au: OK?**][120] and myosin V[73,121] were observed to evaluate the performance of newly developed devices. Recently, HS-AFM provided unique mechanistic insight into the function of bacteriorhodopsin[122], myosin V[123], F_1-ATPase[124], endosomal sorting complex required for transport (ESCRT) III[125] and nuclear pore complexes[126]. HS-AFM images of the light-driven proton pump bacteriorhodopsin showed that on light illumination, the cytoplasmic

E–F helix portion of each bacteriorhodopsin displaces outwards by ~0.7 nm and contacts bacteriorhodopsins from adjacent trimers (Fig. 5f)[122]. Myosin V processively walks along actin filaments in a handover-hand manner, resulting in an ~36 nm step for every adenosine triphosphate (ATP) hydrolysed. HS-AFM observations of myosin V interacting with actin provided a direct observation of the process, and visualized the lever-arm swing, which had been hypothesized for a long time (Fig. 5g)[123]. The results suggested that myosin V steps forward without transitioning through an adenosine diphosphate (ADP)–Pi bound state and, hence, that the actin–myosin binding energy is harnessed to generate the lever-arm swing.

In the rotary motor F_1-ATPase, the γ subunit rotates in the stator $(\alpha\beta)_3$ ring on ATP hydrolysis in the catalytic sites mainly located in the β subunits. This rotation is made possible by rotary propagation of three chemical states (empty, ATP-bound and ADP-bound states) and hence corresponding structural states over the β subunits. HS-AFM visualization of γ-less $(\alpha\beta)_3$ rings revealed that the three states can propagate without the γ subunit (Fig. 5h)[124]. Therefore, the β–β interplay through the α subunits engenders this cooperativity, ruling out a previous γ-dictator model that the cooperativity would be caused by different γ–β interactions for the three β subunits because of an asymmetric structure of the γ subunit.

Sucrose non-fermenting protein 7 (Snf7), an ESCRT-II protein **[Au: OK?]**, plays a key role in lipid membrane budding and abscission. HS-AFM of Snf7 placed on supported planar lipid bilayers showed concentric spiral filaments (Fig. 5i)[125]. On disrupting large spirals with the cantilever tip, the broken polymers spontaneously formed smaller rings, suggesting a preferred diameter of 25 nm for Snf7 as well as 'unbending' of the spiral filaments from their natural curvature. Thus, it was proposed that in cellular conditions, energy would be accumulated during the growth of the spiral spring and eventually released through shrinking of the spiral diameter and buckling of the inner spirals, which would cause the membrane to buckle, bud and abscise.

Nuclear pore complexes (NPCs) facilitate the molecular exchange between cytoplasm and nucleus in eukaryotic cells. However, how nucleoporins form a selective barrier facilitating this transport has been unclear. Applying HS-AFM, it became possible to visualize the spatiotemporal dynamics of nucleoporins inside NPCs of *Xenopus laevis* oocytes at timescales of 100 ms (ref. 126). It was observed that the cytoplasmic orifice is circumscribed by highly flexible, dynamically fluctuating nucleoporins that rapidly elongate and retract. This transient entanglement in the NPC channel manifests as a central plug when averaged in space and time.

Beside these molecular studies, HS-AFM has also been successfully used to observe dynamic processes of live bacteria[127,128] and eukaryotic cells[129]. However, HS-AFM has long relied on scanning the sample stage, which excludes the use of large, heavy sample stages and makes it difficult to combine with optical microscopy. The tip-scan HS-AFM developed very recently will thus significantly expand the applicability to study biological processes by AFM[130]. Observations of **[Au: OK?]**, for example, living cells cultured in Petri dishes, membrane proteins in suspended membranes and proteins responding to external forces applied by optical tweezers will become possible. Cell biological applications, most of which require the combination of AFM and sophisticated optical techniques (see 'Correlative imaging' **[Au: please confirm that this is what was meant by 'next chapter']**, will be made easier. It is also possible to transfer this knowledge to high-speed SICM for studying the dynamics of live cells and isolated intracellular organelles.

Correlative imaging

Living cells present a high level of structural and functional complexity. Cell surfaces consisting of thousands of different macromolecules represent a small heterogeneous and dynamic portion of the cellular complexity. It is thus challenging to identify even simple cell surface structures, such as receptors, channels, transporters and assemblies thereof, in topographs recorded by AFM. In such cases, the full potential of AFM is achieved in combination with complementary microscopy techniques that can identify and correlate complex cellular structures of interest[9]. These complementary techniques include optical microscopy, fluorescence microscopy, confocal microscopy, Förster resonance energy transfer, total internal reflection fluorescence **[Au: OK?]** and super-resolution microscopy. In most cases, AFM has been adapted to fit to optical microscopes. Environmental chambers allowing cellular systems to be kept in their close-to-native state had to be engineered (Fig. 6a). Nowadays, such multimicroscopic combinations allow the unique characterization of a wide range of complex biological systems ranging from membranes and cells to tissues.

A popular combination of AFM is either with epifluorescence or confocal microscopy. Exciting applications range from single animal cells, to tissues and microbial cells, and to their assemblies **[Au: OK?]**. In such studies, structures of interests were fluorescently labelled, optically imaged at micrometre resolution and correlated to AFM topographs contoured at nanometre precision. These approaches identified hitherto unknown supramolecular assemblies of cell surface structures and contributed to the understanding of their function. For example, various steps of the interaction between fungal pathogens and macrophages were captured, including initial cellular contact, fungal cell internalization and hyphal elongation resulting in membrane piercing and escape from the macrophage. While fluorescence imaging distinguished fungal cells from macrophages, AFM revealed biologically relevant nanostructures on both cell types (Fig. 6b,c)[131]. AFM has also been used to image cell surface structures, including microvilli, actin ridges and nanodomains of cellular membranes, and to characterize their dynamic mechanical properties (Fig. 6d)[98,132,133]. Optical microscopy is frequently applied to characterize cell morphology and state while employing AFM to characterize the mechanical properties (for example, stiffness, elasticity, pressure) of the cell or its mechanical interaction (for example, adhesion, migration) with the environment[9]. Such experiments allowed the furrow stiffening during cell division[67] to be observed, the adhesion of *Dictyostelium discoideum* to their substrate to be measured to molecular scale[134] and whether cell adhesion or cortex tension determine cell sorting in the developing embryo to be unravelled[135]. Importantly, some of the experiments contributed answers to a controversial debate lasting for more than three decades. Combined AFM and confocal microscopy was used to monitor the angiotensin-induced contractile response and cytoskeleton remodelling in human embryonic kidney cells[136]. Other examples used confocal microscopy to monitor eukaryotic cells transiently expressing green fluorescent protein–actin, tubulin, vimentin and LaminA, and imaged the mechanical properties of the cytoskeleton and nucleus during early apoptosis[137]. AFM was also applied to measure the cell pressure and cortex tension while quantifying the actin and myosin accumulating at the cell cortex by confocal microscopy (Fig. 6e–h) **[Au: please confirm that the addition of panel h to this citation is correct]**[138]. This approach contributed to the understanding of how adherent animal cells facilitate and regulate their rather drastic cell shape changes required to progress through mitosis[139].

As discussed above, cantilevers functionalized with biological molecules, chemical groups or even with living cells can reveal specific sites and their interactions on live cells[9]. Applying molecular recognition AFM in conjunction with optical microscopy can reveal a comprehensive picture of the distribution of cell surface receptors and of cell morphology and state. Recent examples include the localization of receptors on CHO cells and endothelial cells[140], and the visualization of the peptidoglycan insertion into the cell

wall of *Lactococcus lactis*[50] while mapping the distribution of single peptidoglycan molecules on the outermost cell surface using AFM. Molecular recognition AFM and fluorescence microscopy also linked the spatial localization and functional role of cell wall teichoic acids in *Lactobacillus plantarum*[100]. Polarized cell-wall organization was found to play a key role in controlling cell morphogenesis. In yeast, both AFM recognition imaging and confocal microscopy demonstrated that agglutinin-like sequence adhesion proteins form nanodomains on live cells through amyloid interactions[141]. Very recently, AFM tips functionalized with single rabies viruses were used to correlate fluorescence images of cell surface receptors to viral binding events to the animal cell[142]. Analysis of the initial binding events revealed that the viral glycoproteins bind cell surface receptors in an allosteric mode until all three binding sites of the trimeric cell surface receptor are occupied and viral fusion can be initiated.

Conclusions

A wealth of AFM imaging modes have been developed to provide multiparametric and multifunctional characterization of biological systems. These methods include the high-resolution imaging of native biostructures and the simultaneous mapping of mechanical, kinetic and thermodynamic properties, of functional groups and binding sites, of free energy landscapes of ligand-receptor bonds, and of electrostatic properties ranging from charge distributions to ion currents. In recent years, many new AFM imaging modes have been developed, which in principle can be readily applied to biological systems and thus will further extend the variety of information that can be quantified and structurally mapped while imaging complex biological systems. At present, the force sensitivity and thermal stability (drift) of AFM limit the precision at which biological systems can be characterized. Therefore, recently introduced ultrastable AFMs, which provide subpiconewton force precision and high positional stability (<0.03 Å) at extremely low lateral drift (~5 pm min^{-1})[143,144], could potentially be the basis for the development of AFMs for new applications of biological significance. Furthermore, most bio-AFM users currently apply single AFM-imaging modes in their specific field of interest. However, biological systems are complex and require a range of information to be understood. Therefore, we expect that many of the AFM modes discussed here will soon be combined into one instrument and thus into one set of correlated measurements. Such multimodal, multiparametric, multifrequency and high-speed AFM imaging platforms should lead to a more comprehensive understanding of the dynamic, structural, mechanical, chemical and functional heterogeneity of complex biological systems. Together with advances in complementary techniques (Table 1), this will allow AFM to address outstanding questions in biology in the coming decades.

Received 10 June 2016; accepted 23 February 2017; published online 6 April 2017

References [Au: please check/confirm queries in the refs list]

1. Binnig, G., Quate, C. F. & Gerber, C. Atomic force microscope. *Phys. Rev. Lett.* **56,** 930–933 (1986). **This paper first described the principles of AFM.**
2. Gerber, C. & Lang, H. P. How the doors to the nanoworld were opened. *Nat. Nanotech.* **1,** 3–5 (2006).
3. Binnig, G., Gerber, C., Stoll, E., Albrecht, T. R. & Quate, C. F. Atomic resolution with atomic force microscope. *Europhys. Lett.* **3,** 1281–1286 (1987).
4. Drake, B. *et al.* Imaging crystals, polymers, and processes in water with the atomic force microscope. *Science* **243,** 1586–1589 (1989).
5. Radmacher, M., Tillmann, R. W. & Gaub, H. E. Imaging viscoelasticity by force modulation with the atomic force microscope. *Biophys. J.* **64,** 735–742 (1993).
6. Horber, J. K. & Miles, M. J. Scanning probe evolution in biology. *Science* **302,** 1002–1005 (2003).
7. Binnig, G. & Rohrer, H. In touch with atoms. *Rev. Mod. Phys.* **71,** S324 (1999). **[Au: please provide page range or confirm single-page reference or article number]**
8. Muller, D. J. & Dufrene, Y. F. Atomic force microscopy as a multifunctional molecular toolbox in nanobiotechnology. *Nat. Nanotech.* **3,** 261–269 (2008).
9. Muller, D. J., Helenius, J., Alsteens, D. & Dufrene, Y. F. Force probing surfaces of living cells to molecular resolution. *Nat. Chem. Biol.* **5,** 383–390 (2009).
10. Hansma, H. G. & Hoh, J. H. Biomolecular imaging with the atomic force microscope. *Annu. Rev. Biophys. Biomol. Struct.* **23,** 115–139 (1994).
11. Hinterdorfer, P. & Dufrene, Y. F. Detection and localization of single molecular recognition events using atomic force microscopy. *Nat. Methods* **3,** 347–355 (2006).
12. Ando, T., Uchihashi, T. & Kodera, N. High-speed AFM and applications to biomolecular systems. *Ann. Rev. Biophys.* **42,** 393–414 (2013).
13. Dufrene, Y. F., Martinez-Martin, D., Medalsy, I., Alsteens, D. & Muller, D. J. Multiparametric imaging of biological systems by force-distance curve–based AFM. *Nat. Methods* **10,** 847–854 (2013).
14. Garcia, R. & Proksch, R. Nanomechancial mapping of soft matter by bimodal force microscopy. *Eur. Polym. J.* **49,** 1897–1906 (2013).
15. Radmacher, M., Tillmann, R. W., Fritz, M. & Gaub, H. E. From molecules to cells: imaging soft samples with the atomic force microscope. *Science* **257,** 1900–1905 (1992).
16. Henderson, E., Haydon, P. G. & Sakaguchi, D. S. Actin filament dynamics in living glial cells imaged by atomic force microscopy. *Science* **257,** 1944–1946 (1992).
17. Hoh, J. H. & Schoenenberger, C. A. Surface morphology and mechanical properties of MDCK monolayers by atomic force microscopy. *J. Cell Sci.* **107,** 1105–1114 (1994).
18. Hoh, J. H., Lal, R., John, S. A., Revel, J.-P. & Arnsdorf, M. F. Atomic force microscopy and dissection of gap junctions. *Science* **253,** 1405–1408 (1991).
19. Mou, J., Yang, J. & Shao, Z. Atomic force microscopy of cholera toxin B-oligomers bound to bilayers of biologically relevant lipids. *J. Mol. Biol.* **248,** 507–512 (1995).
20. Schabert, F. A., Henn, C. & Engel, A. Native *Escherichia coli* OmpF porin surfaces probed by atomic force microscopy. *Science* **268,** 92–94 (1995).
21. Hansma, H. G. *et al.* Reproducible imaging and dissection of plasmid DNA under liquid with the atomic force microscope. *Science* **256,** 1180–1184 (1992).
22. Egger, M. *et al.* Wet lipid protein membranes imaged at submolecular resolution by atomic force microscopy. *J. Struct. Biol.* **103,** 89–94 (1990).
23. Zasadzinski, J. A., Viswanathan, R., Madsen, L., Garnaes, J. & Schwartz, D. K. Langmuir-Blodgett films. *Science* **263,** 1726–1733 (1994).
24. Yang, J., Mou, J. X. & Shao, Z. F. Structure and stability of pertussis toxin studied by *in situ* atomic force microscopy. *FEBS Lett.* **338,** 89–92 (1994).
25. Müller, D. J., Schabert, F. A., Büldt, G. & Engel, A. Imaging purple membranes in aqueous solutions at sub-nanometer resolution by atomic force microscopy. *Biophys. J.* **68,** 1681–1686 (1995).
26. Müller, D. J., Engel, A., Carrascosa, J. & Veléz, M. The bacteriophage ø29 head–tail connector imaged at high resolution with atomic force microscopy in buffer solution. *EMBO J.* **16,** 2547–2553 (1997).
27. Czajkowsky, D. M., Sheng, S. & Shao, Z. Staphylococcal alpha-hemolysin can form hexamers in phospholipid bilayers. *J. Mol. Biol.* **276,** 325–330 (1998).
28. Seelert, H. *et al.* Proton powered turbine of a plant motor. *Nature* **405,** 418–419 (2000).
29. Scheuring, S., Reiss-Husson, F., Engel, A., Rigaud, J. L. & Ranck, J. L. High-resolution AFM topographs of *Rubrivivax gelatinosus* light- harvesting complex LH2. *EMBO J.* **20,** 3029–3035 (2001).
30. Fotiadis, D. *et al.* Atomic-force microscopy: rhodopsin dimers in native disc membranes. *Nature* **421,** 127–128 (2003).
31. Goldsbury, C., Kistler, J., Aebi, U., Arvinte, T. & Cooper, G. J. Watching amyloid fibrils grow by time-lapse atomic force microscopy. *J. Mol. Biol.* **285,** 33–39 (1999).
32. Bezanilla, M. *et al.* Motion and enzymatic degradation of DNA in the atomic force microscope. *Biophys. J.* **67,** 2454–2459 (1994).
33. Grandbois, M., Clausen-Schaumann, H. & Gaub, H. Atomic force microscope imaging of phospholipid bilayer degradation by phospholipase A2. *Biophys. J.* **74,** 2398–2404 (1998).
34. Muller, D. J. & Engel, A. Voltage and pH-induced channel closure of porin OmpF visualized by atomic force microscopy. *J. Mol. Biol.* **285,** 1347–1351 (1999).
35. Müller, D. J., Hand, G. M., Engel, A. & Sosinsky, G. Conformational changes in surface structures of isolated connexin 26 gap junctions. *EMBO J.* **21,** 3598–3607 (2002). **This paper reports using AFM to image animal communication channels at work with high-resolution.**
36. Stoffler, D., Goldie, K. N., Feja, B & Aebi, U. Calcium-mediated structural changes of native nuclear pore complexes monitored by time-lapse atomic force microscopy. *J. Mol. Biol.* **287,** 741–752 (1999).
37. Czajkowsky, D. M., Hotze, E. M., Shao, Z. & Tweten, R. K. Vertical collapse of a cytolysin prepore moves its transmembrane beta-hairpins to the membrane. *EMBO J.* **23,** 3206–3215 (2004).
38. Scheuring, S. & Sturgis, J. N. Chromatic adaptation of photosynthetic membranes. *Science* **309,** 484–487 (2005).

39. Engel, A. & Muller, D. J. Observing single biomolecules at work with the atomic force microscope. *Nat. Struct. Biol.* **7,** 715–718 (2000).
40. Albrecht, T. R., Grutter, P., Horne, D. & Rugar, D. Frequency-modulation detection using high-*Q* cantilevers for enhanced force microscope sensitivity. *J. Appl. Phys.* **69,** 668–673 (1991).
41. Putman, C. A. J., Vanderwerf, K. O., Degrooth, B. G., Vanhulst, N. F. & Greve, J. Tapping mode atomic-force microscopy in liquid. *Appl. Phys. Lett.* **64,** 2454–2456 (1994).
42. Garcia, R. & Herruzo, E. T. The emergence of multifrequency force microscopy. *Nat. Nanotech.* **7,** 217–226 (2012). **A review describing recent progress in multifrequency force microscopy, and discussing its potential for studying proteins and cells.**
43. Hansma, P. K. *et al.* Tapping mode atomic-force microscopy in liquids. *Appl. Phys. Lett.* **64,** 1738–1740 (1994).
44. Wegmann, S. *et al.* Human Tau isoforms assemble into ribbon-like fibrils that display polymorphic structure and stability. *J. Biol. Chem.* **285,** 27302–27313 (2010).
45. Ido, S. *et al.* Beyond the helix pitch: direct visualization of native DNA in aqueous solution. *ACS Nano* **7,** 1817–1822 (2013).
46. Ido, S. *et al.* Immunoactive two-dimensional self-assembly of monoclonal antibodies in aqueous solution revealed by atomic force microscopy. *Nat. Mater.* **13,** 264–270 (2014).
47. Möller, C., Allen, M., Elings, V., Engel, A. & Müller, D. J. Tapping mode atomic force microscopy produces faithful high-resolution images of protein surfaces. *Biophys. J.* **77,** 1050–1058 (1999).
48. Stark, M., Moller, C., Muller, D. J. & Guckenberger, R. From images to interactions: high-resolution phase imaging in tapping-mode atomic force microscopy. *Biophys. J.* **80,** 3009–3018 (2001).
49. Kasas, S. & Ikai, A. A method for anchoring round shaped cells for atomic force microscope imaging. *Biophys. J.* **68,** 1678–1680 (1995).
50. Andre, G. *et al.* Imaging the nanoscale organization of peptidoglycan in living *Lactococcus lactis* cells. *Nat. Commun.* **1,** 27 (2010).
51. Hansma, P. K., Drake, B., Marti, O., Gould, S. A. & Prater, C. B. The scanning ion-conductance microscope. *Science* **243,** 641–643 (1989).
52. Novak, P. *et al.* Nanoscale live-cell imaging using hopping probe ion conductance microscopy. *Nat. Methods* **6,** 279–281 (2009).
53. Drake, B., Randall, C., Bridges, D. & Hansma, P. K. A new ion sensing deep atomic force microscope. *Rev. Sci. Instrum.* **85,** 083706 (2014).
54. Roos, W. H., Bruinsma, R. & Wuite, G. J. L. Physical virology. *Nat. Phys.* **6,** 733–743 (2010).
55. Oesterhelt, F. *et al.* Unfolding pathways of individual bacteriorhodopsins. *Science* **288,** 143–146 (2000).
56. Kufer, S. K., Puchner, E. M., Gumpp, H., Liedl, T. & Gaub, H. E. Single-molecule cut-and-paste surface assembly. *Science* **319,** 594–596 (2008).
57. Braunschweig, A. B., Huo, F. & Mirkin, C. A. Molecular printing. *Nat. Chem.* **1,** 353–358 (2009).
58. Cattin, C. J. *et al.* Mechanical control of mitotic progression in single animal cells. *Proc. Natl Acad. Sci. USA* **112,** 11258–11263 (2015).
59. Butt, H. J., Cappella, B. & Kappl, M. Force measurements with the atomic force microscope: technique, interpretation and applications. *Surf. Sci. Rep.* **59,** 1–152 (2005).
60. Dong, M., Husale, S. & Sahin, O. Determination of protein structural flexibility by microsecond force spectroscopy. *Nat. Nanotech.* **4,** 514–517 (2009).
61. Martinez-Martin, D., Herruzo, E. T., Dietz, C., Gomez-Herrero, J. & Garcia, R. Noninvasive protein structural flexibility mapping by bimodal dynamic force microscopy. *Phys. Rev. Lett.* **106,** 198101 (2011).
62. Herruzo, E. T., Perrino, A. P. & Garcia, R. Fast nanomechanical spectroscopy of soft matter. *Nat. Commun.* **5,** 3126 (2014).
63. Preiner, J. *et al.* High-speed AFM images of thermal motion provide stiffness map of interfacial membrane protein moieties. *Nano Lett.* **15,** 759–763 (2015).
64. Radmacher, M., Cleveland, J. P., Fritz, M., Hansma, H. G. & Hansma, P. K. Mapping interaction forces with the atomic force microscope. *Biophys. J.* **66,** 2159–2165 (1994).
65. Heinz, W. F. & Hoh, J. H. Spatially resolved force spectroscopy of biological surfaces using the atomic force microscope. *Trends Biotechnol.* **17,** 143–150 (1999).
66. Rotsch, C. & Radmacher, M. Drug-induced changes of cytoskeletal structure and mechanics in fibroblasts: an atomic force microscopy study. *Biophys. J.* **78,** 520–535 (2000).
67. Matzke, R., Jacobson, K. & Radmacher, M. Direct, high-resolution measurement of furrow stiffening during division of adherent cells. *Nat. Cell Biol.* **3,** 607–610 (2001).
68. Plodinec, M. *et al.* The nanomechanical signature of breast cancer. *Nat. Nanotech.* **7,** 757–765 (2012).
69. Rebelo, L. M., de Sousa, J. S., Mendes Filho, J. & Radmacher, M. Comparison of the viscoelastic properties of cells from different kidney cancer phenotypes measured with atomic force microscopy. *Nanotechnology* **24,** 055102 (2013).
70. Touhami, A., Nysten, B. & Dufrêne, Y. F. Nanoscale mapping of the elasticity of microbial cells by atomic force microscopy. *Langmuir* **19,** 4539–4543 (2003).
71. Viani, M. B. *et al.* Fast imaging and fast force spectroscopy of single biopolymers with a new atomic force microscope designed for small cantilevers. *Rev. Sci. Instrum.* **70,** 4300–4303 (1999). **This paper reports the invention of small cantilevers for fast AFM imaging and force spectroscopy.**
72. Viani, M. B. *et al.* Small cantilevers for force spectroscopy of single molecules. *J. Appl. Phys.* **86,** 2258–2262 (1999).
73. Ando, T. *et al.* A high-speed atomic force microscope for studying biological macromolecules. *Proc. Natl Acad. Sci. USA* **98,** 12468–12472 (2001).
74. Alcaraz, J. *et al.* Correction of microrheological measurements of soft samples with atomic force microscopy for the hydrodynamic drag on the cantilever. *Langmuir* **18,** 716–721 (2002).
75. Sahin, O., Magonov, S., Su, C., Quate, C. F. & Solgaard, O. An atomic force microscope tip designed to measure time-varying nanomechanical forces. *Nat. Nanotech.* **2,** 507–514 (2007).
76. Medalsy, I., Hensen, U. & Muller, D. J. Imaging and quantifying chemical and physical properties of native proteins at molecular resolution by force-volume AFM. *Angew. Chem. Int. Ed.* **50,** 12103–12108 (2011).
77. Sullan, R. M., Li, J. K. & Zou, S. Direct correlation of structures and nanomechanical properties of multicomponent lipid bilayers. *Langmuir* **25,** 7471–7477 (2009).
78. Heu, C., Berquand, A., Elie-Caille, C. & Nicod, L. Glyphosate-induced stiffening of HaCaT keratinocytes, a Peak Force Tapping study on living cells. *J. Struct. Biol.* **178,** 1–7 (2012).
79. Formosa-Dague, C., Speziale, P., Foster, T. J., Geoghegan, J. A. & Dufrene, Y. F. Zinc-dependent mechanical properties of *Staphylococcus aureus* biofilm-forming surface protein SasG. *Proc. Natl Acad. Sci. USA* **113,** 410–415 (2016).
80. Alsteens, D., Trabelsi, H., Soumillion, P. & Dufrene, Y. F. Multiparametric atomic force microscopy imaging of single bacteriophages extruding from living bacteria. *Nat. Commun.* **4,** 2926 (2013).
81. Carrasco, C. *et al.* Built-in mechanical stress in viral shells. *Biophys. J.* **100,** 1100–1108 (2011).
82. Zink, M. & Grubmuller, H. Mechanical properties of the icosahedral shell of southern bean mosaic virus: a molecular dynamics study. *Biophys. J.* **96,** 1350–1363 (2009).
83. Carrasco, C. *et al.* DNA-mediated anisotropic mechanical reinforcement of a virus. *Proc. Natl Acad. Sci. USA* **103,** 13706–13711 (2006).
84. Alsteens, D., Garcia, M. C., Lipke, P. N. & Dufrene, Y. F. Force-induced formation and propagation of adhesion nanodomains in living fungal cells. *Proc. Natl Acad. Sci. USA* **107,** 20744–20749 (2010). **This paper reports using recognition imaging to demonstrate that microbial cell adhesion proteins form nanoclusters under mechanical force.**
85. Pfreundschuh, M., Hensen, U. & Muller, D. J. Quantitative imaging of the electrostatic field and potential generated by a transmembrane protein pore at subnanometer resolution. *Nano Lett.* **13,** 5585–5593 (2013).
86. Evans, E. A. & Calderwood, D. A. Forces and bond dynamics in cell adhesion. *Science* **316,** 1148–1153 (2007).
87. Medalsy, I. D. & Muller, D. J. Nanomechanical properties of proteins and membranes depend on loading rate and electrostatic interactions. *ACS Nano* **7,** 2642–2650 (2013).
88. Frisbie, C. D., Rozsnyai, L. F., Noy, A., Wrighton, M. S. & Lieber, C. M. Functional group imaging by chemical force microscopy. *Science* **265,** 2071–2074 (1994).
89. Hinterdorfer, P., Baumgartner, W., Gruber, H. J., Schilcher, K. & Schindler, H. Detection and localization of individual antibody-antigen recognition events by atomic force microscopy. *Proc. Natl Acad. Sci. USA* **93,** 3477–3481 (1996).
90. Ludwig, M., Dettmann, W. & Gaub, H. E. Atomic force microscope imaging contrast based on molecular recognition. *Biophys. J.* **72,** 445–448 (1997).
91. Grandbois, M., Dettmann, W., Benoit, M. & Gaub, H. E. Affinity imaging of red blood cells using an atomic force microscope. *J. Histochem. Cytochem.* **48,** 719–724 (2000).
92. Florin, E. L., Moy, V. T. & Gaub, H. E. Adhesion forces between individual ligand-receptor pairs. *Science* **264,** 415–417 (1994).
93. Lee, G. U., Chrisey, L. A. & Colton, R. J. Direct measurement of the forces between complementary strands of DNA. *Science* **266,** 771–773 (1994).
94. Kienberger, F. *et al.* Recognition force spectroscopy studies of the NTA-His6 bond. *Single Mol.* **1,** 59–65 (2000).
95. Thie, M. *et al.* Interactions between trophoblast and uterine epithelium: monitoring of adhesive forces. *Hum. Reprod.* **13,** 3211–3219 (1998).
96. Kim, H., Arakawa, H., Osada, T. & Ikai, A. Quantification of cell adhesion force with AFM: distribution of vitronectin receptors on a living MC3T3-E1 cell. *Ultramicroscopy* **97,** 359–363 (2003).
97. Kim, H. *et al.* Quantification of the number of EP3 receptors on a living CHO cell surface by the AFM. *Ultramicroscopy* **106,** 652–662 (2006).

98. Roduit, C. *et al.* Elastic membrane heterogeneity of living cells revealed by stiff nanoscale membrane domains. *Biophys. J.* **94,** 1521–1532 (2008).
99. Alsteens, D. *et al.* Imaging G protein–coupled receptors while quantifying their ligand-binding free-energy landscape. *Nat. Methods* **12,** 845–851 (2015). **This paper showed that attaching a ligand to the AFM stylus allows it to image and map its binding to human G protein–coupled receptors and to reconstruct the ligand-binding free-energy landscape.**
100. Andre, G. *et al.* Fluorescence and atomic force microscopy imaging of wall teichoic acids in *Lactobacillus plantarum*. *ACS Chem. Biol.* **6,** 366–376 (2011).
101. Dupres, V. *et al.* Nanoscale mapping and functional analysis of individual adhesins on living bacteria. *Nat. Methods* **2,** 515–520 (2005). **This paper reports that AFM tips labelled with bioligands can map the distribution of single adhesion proteins on bacterial pathogens and reveal their assembly into nanodomains.**
102. Pfreundschuh, M. *et al.* Identifying and quantifying two ligand-binding sites while imaging native human membrane receptors by AFM. *Nat. Commun.* **6,** 8857 (2015).
103. Raab, A. *et al.* Antibody recognition imaging by force microscopy. *Nat. Biotechnol.* **17,** 901–905 (1999).
104. Stroh, C. *et al.* Single-molecule recognition imaging microscopy. *Proc. Natl Acad. Sci. USA* **101,** 12503–12507 (2004).
105. Chtcheglova, L. A., Waschke, J., Wildling, L., Drenckhahn, D. & Hinterdorfer, P. Nano-scale dynamic recognition imaging on vascular endothelial cells. *Biophys. J.* **93,** L11–L13 (2007).
106. Zhang, S., Aslan, H., Besenbacher, F. & Dong. M. Quantitative biomolecular imaging by dynamic nanomechanical mapping. *Chem. Soc. Rev.* **43,** 7412–7429 (2014).
107. Dietz, C., Herruzo, E. T., Lozano, J. R. & Garcia, R. Nanomechanical coupling enables detection and imaging of 5 nm superparamagnetic particles in liquid. *Nanotechnology* **22,** 125708 (2011).
108. Herruzo, E. T., Asakawa, H., Fukuma, T. & Garcia, R. Three-dimensional quantitative force maps in liquid with 10 piconewton, angstrom and sub-minute resolutions. *Nanoscale* **5,** 2678–2685 (2013).
109. Fukuma, T., Higgins, M. J. & Jarvis, S. P. Direct imaging of individual intrinsic hydration layers on lipid bilayers at Angstrom resolution. *Biophys. J.* **92,** 3603–3609 (2007).
110. Cartagena, A., Hernando-Perez, M., Carrascosa, J. L., de Pablo, P. J. & Raman, A. Mapping *in vitro* local material properties of intact and disrupted virions at high resolution using multi-harmonic atomic force microscopy. *Nanoscale* **5,** 4729–4736 (2013).
111. Cartagena-Rivera, A. X., Wang, W. H., Geahlen, R. L. & Raman, A. Fast, multi-frequency, and quantitative nanomechanical mapping of live cells using the atomic force microscope. *Sci. Rep.* **5,** 11692 (2015).
112. Kim, D. & Sahin, O. Imaging and three-dimensional reconstruction of chemical groups inside a protein complex using atomic force microscopy. *Nat. Nanotech.* **10,** 264–269 (2015).
113. Shekhawat, G. S. & Dravid, V. P. Nanoscale imaging of buried structures via scanning near-field ultrasound holography. *Science* **310,** 89–92 (2005).
114. Tetard, L. *et al.* Imaging nanoparticles in cells by nanomechanical holography. *Nat. Nanotech.* **3,** 501–505 (2008).
115. Verbiest, G. J. & Rost, M. J. Beating beats mixing in heterodyne detection schemes. *Nat. Commun.* **6,** 6444 (2015).
116. Kindt, J. H., Fantner, G. E., Cutroni, J. A. & Hansma, P. K. Rigid design of fast scanning probe microscopes using finite element analysis. *Ultramicroscopy* **100,** 259–265 (2004).
117. Ando, T., Uchihashi, T. & Fukuma, T. High-speed atomic force microscopy for nano-visualization of dynamic biomolecular processes. *Prog. Surf. Sci.* **83,** 337–437 (2008).
118. Kodera, M., Yamashita, H. & Ando, T. Active damping of the scanner for high-speed atomic force microscopy. *Rev. Sci. Instrum.* **76,** 053708 (2005).
119. Kodera, N., Sakashita, M. & Ando, T. Dynamic proportional-integral-differential controller for high-speed atomic force microscopy. *Rev. Sci. Instrum.* **77,** 083704 (2006).
120. Viani, M. B. *et al.* Probing protein–protein interactions in real time. *Nat. Struct. Biol.* **7,** 644–647 (2000).
121. Ando, T. *et al.* A high-speed atomic force microscope for studying biological macromolecules in action. *ChemPhysChem* **4,** 1196–1202 (2003).
122. Shibata, M., Yamashita, H., Uchihashi, T., Kandori, H. & Ando, T. High-speed atomic force microscopy shows dynamic molecular processes in photoactivated bacteriorhodopsin. *Nat. Nanotech.* **5,** 208–212 (2010).
123. Kodera, N., Yamamoto, D., Ishikawa, R. & Ando, T. Video imaging of walking myosin V by high-speed atomic force microscopy. *Nature* **468,** 72–76 (2010). **This paper showed that high-speed AFM can be used to watch proteins functioning in real-time.**
124. Uchihashi, T., Iino, R., Ando, T. & Noji, H. High-speed atomic force microscopy reveals rotary catalysis of rotorless F(1)-ATPase. *Science* **333,** 755–758 (2011).
125. Chiaruttini, N. *et al.* Relaxation of loaded ESCRT-III spiral springs drives membrane deformation. *Cell* **163,** 866–879 (2015).
126. Sakiyama, Y., Mazur, A., Kapinos, L. E. & Lim, R. Y. Spatiotemporal dynamics of the nuclear pore complex transport barrier resolved by high-speed atomic force microscopy. *Nat. Nanotech.* **11,** 719–723 (2016).
127. Fantner, G. E., Barbero, R. J., Gray, D. S. & Belcher, A. M. Kinetics of antimicrobial peptide activity measured on individual bacterial cells using high-speed atomic force microscopy. *Nat. Nanotech.* **5,** 280–285 (2010).
128. Yamashita, H. *et al.* Single-molecule imaging on living bacterial cell surface by high-speed AFM. *J. Mol. Biol.* **422,** 300–309 (2012).
129. Shibata, M., Uchihashi, T., Ando, T. & Yasuda, R. Long-tip high-speed atomic force microscopy for nanometer-scale imaging in live cells. *Sci. Rep.* **5,** 8724 (2015).
130. Uchihashi, T., Watanabe, H., Fukuda, S., Shibata, M. & Ando, T. Functional extension of high-speed AFM for wider biological applications. *Ultramicroscopy* **160,** 182–196 (2016).
131. El-Kirat-Chatel, S. & Dufrene, Y. F. Nanoscale imaging of the *Candida* — macrophage interaction using correlated fluorescence-atomic force microscopy. *ACS Nano* **6,** 10792–10799 (2012).
132. Sharma, A., Anderson, K. & Muller, D. J. Actin microridges characterized by laser scanning confocal and atomic force microscopy. *FEBS Lett.* **579,** 2001–2009 (2005).
133. Schillers, H., Medalsy, I., Hu, S., Slade, A. L. & Shaw, J. E. PeakForce Tapping resolves individual microvilli on living cells. *J. Mol. Recognit.* **29,** 95–101 (2016).
134. Benoit, M., Gabriel, D., Gerisch, G. & Gaub, H. E. Discrete interactions in cell adhesion measured by single-molecule force spectroscopy. *Nat. Cell Biol.* **2,** 313–317 (2000).
135. Krieg, M. *et al.* Tensile forces govern germ-layer organization in zebrafish. *Nat. Cell Biol.* **10,** 429–436 (2008).
136. Cuerrier, C. M., Gagner, A., Lebel, R., Gobeil, F. Jr & Grandbois, M. Effect of thrombin and bradykinin on endothelial cell mechanical properties monitored through membrane deformation. *J. Mol. Recognit.* **22,** 389–396 (2009).
137. Pelling, A. E., Veraitch, F. S., Chu, C. P., Mason, C. & Horton, M. A. Mechanical dynamics of single cells during early apoptosis. *Cell Motil. Cytoskel.* **66,** 409–422 (2009).
138. Ramanathan, S. P. *et al.* Cdk1-dependent mitotic enrichment of cortical myosin II promotes cell rounding against confinement. *Nat. Cell Biol.* **17,** 148–159 (2015).
139. Stewart, M. P. *et al.* Hydrostatic pressure and the actomyosin cortex drive mitotic cell rounding. *Nature* **469,** 226–230 (2011).
140. Duman, M. *et al.* Improved localization of cellular membrane receptors using combined fluorescence microscopy and simultaneous topography and recognition imaging. *Nanotechnology* **21,** 115504 (2010).
141. Lipke, P. N. *et al.* Strengthening relationships: amyloids create adhesion nanodomains in yeasts. *Trends Microbiol.* **20,** 59–65 (2012).
142. Alsteens, D. *et al.* Nanomechanical mapping of first binding steps of a virus to animal cells. *Nat. Nanotech.* **12,** 177–183 (2017). **This paper showed that attaching a rabies virus to the AFM stylus allows living animal cells to be imaged with confocal microscopy and AFM, to simultaneously localize virus-binding, and to quantify the virus-binding process and free-energy landscape.** **[Au: please confirm volume number, page range and year are correct as added]**
143. Churnside, A. B. & Perkins, T. T. Ultrastable atomic force microscopy: improved force and positional stability. *FEBS Lett.* **588,** 3621–3630 (2014).
144. King, G. M., Carter, A. R., Churnside, A. B., Eberle, L. S. & Perkins, T. T. Ultrastable atomic force microscopy: atomic-scale stability and registration in ambient conditions. *Nano Lett.* **9,** 1451–1456 (2009).
145. Franz, C. M. & Muller, D. J. Analysing focal adhesion structure by AFM. *J. Cell Sci.* **118,** 5315–5323 (2005).
146. Lucas, R. W., Kuznetsov, Y. G., Larson, S. B. & McPherson, A. Crystallization of Brome mosaic virus and T = 1 Brome mosaic virus particles following a structural transition. *Virology* **286,** 290–303 (2001).
147. Friedrichs, J., Taubenberger, A., Franz, C. M. & Muller, D. J. Cellular remodelling of individual collagen fibrils visualized by time-lapse AFM. *J. Mol. Biol.* **372,** 594–607 (2007).
148. Mari, S. A. *et al.* Gating of the MlotiK1 potassium channel involves large rearrangements of the cyclic nucleotide-binding domains. *Proc. Natl Acad. Sci. USA* **108,** 20802–20807 (2011).
149. Bestembayeva, A. *et al.* Nanoscale stiffness topography reveals structure and mechanics of the transport barrier in intact nuclear pore complexes. *Nat. Nanotech.* **10,** 60–64 (2015).
150. Dietz, C. *et al.* Nanotomography with enhanced resolution using bimodal atomic force microscopy. *Appl. Phys. Lett.* **92,** 143107 (2008).

Acknowledgements

Y.F.D. was supported by the Université catholique de Louvain, the European Research Council (ERC) under the European Union's Horizon 2020 research and innovation programme (grant agreement no. 693630), the WELBIO (grant n°WELBIO-CR-2015A-05), the National Fund for Scientific Research (FNRS), the Federal Office for Scientific, Technical and Cultural Affairs (Interuniversity Poles of Attraction Programme) and the Research Department of the Communauté française de Belgique (Concerted Research Action). D.A. and D.M.M. were supported by the European Molecular Biology Organization (EMBO; ALTF 265-2013 and ALTF 506-2012). D.J.M. was supported by the Swiss National Science Foundation (SNF; grant 310030B_160225), the NCCR Molecular Systems Engineering and the Swiss Commission for Technology and Innovation (CTI; grant 17970.1). R.G. acknowledges financial support from the European Research Council AdG no. 340177 and the Ministerio de Economia y Competitividad MAT2016-76507-R. T.A. was supported by the Japan Society for the Promotion of Science (JSPS; grants 24227005 and 26119003) and by the Japan Science and Technology Agency (JST; CREST program on Structural Life Science and Advanced Core Technology for Innovative Life Science Research).

Additional information

 Correspondence should be addressed to Y.F.D and D.J.M.

Competing financial interests

The authors declare no competing financial interests.